Indian J. Phys. **81 (10)** 969-981 (2007)

IJP

Aspects of electron dynamics in a helium atom under an intense laser field

Mainak Sadhukhan[1] and B M Deb[2]*

[1]S N Bose National Centre for Basic Sciences JD Block Sector III, Salt Lake Kolkata 700 098, India

[2]Indian Institute of Science Education & Research, HC VII, Sector III Salt Lake, Kolkata 700 106, India

E-mail bmdeb@yahoo co in

Received 12 September 2007 accepted 16 September 2007

Abstract : Aspects of the dynamics of electrons in a helium atom interacting with an intense laser of intensity 1×10^{15} W cm^{-2} over a time of 100 fs are theoretically studied through a single time-dependent generalized nonlinear Schrodinger equation (GNLSE) of motion The GNLSE was derived earlier by combining time-dependent (TD) density functional theory and quantum fluid dynamics It has been solved fully numerically to yield results on the TD number of electrons, electron density changes, oscillating induced dipole moment, *etc* The method can reveal attosecond changes in the electron density as well as create an attosecond laser pulse, of peak intensity 10^9 W cm^{-2}, out of the generated high-order harmonics The method goes beyond the linear-response formalisms and, in principle, calculates density to all orders of change.

Keywords : Time-dependent density functional theory Multi-photon ionization and excitation to highly excited states Strong-field excitation of optical transitions in quantum systems, multi-photon processes, dynamic Stark shift Ultra-fast processes, optical pulse generation and pulse compression

PACS Nos. : 31 15 ee, 32 80 Rm, 42 50.Hz, 42.65 Re

1. Introduction

The strongly driven, non-linear, multi-photon interaction between matter and intense laser fields has received a great deal of attention in the last two decades, through a strong interplay between experimental and theoretical studies [1–5]. Such material systems have included atoms, molecules, condensed matter and plasma. In the case of atoms and molecules, multi-photon processes such as high-order harmonics generation (HHG), above-threshold ionization (ATI), above-threshold dissociation (ATD) of molecules, stabilization under super-intense laser fields, generation of XUV and X-ray laser pulses, *etc.* were observed. These phenomena were realized to be dynamical (time-dependent) consequences of electronic motions in the systems under the intense laser fields.

*Corresponding Author

A many-electron atom – even a two-electron atom like helium – is a "strongly correlated" system The average time scale of a cycle of electronic motion in an atom or molecule is a few hundred attoseconds (1 *as* = 10^{-18} s) For an intense laser (*e g* a petawatt laser of intensity 1 × 10^{15} W cm^{-2}), the strength of the laser electric field is comparable to the strength of the nuclear electric field in which the electrons move in a correlated fashion Therefore, the laser field modifies the internal electronic structure of the system and thereby significantly alters the electron dynamics

Theoretical treatments of intense laser-atom interactions in the petawatt regime should be non-perturbative and include all the physical effects of dynamical interaction between the electrons, *viz*, Coulomb, exchange and correlation A given theoretical method should also be able to reflect changes in the electronic wave function or density over a few hundred attoseconds so that detailed features of electronic motion may be probed By exploiting the high-order harmonics, the method should also be able to generate an attosecond laser pulse [6] Note, however, that calculations on a single system can reproduce the experimental results only qualitatively, the latter being the outcome of non-linear mixing of responses from many systems.

In this paper, we apply a formalism based on time-dependent density-functional theory (TDDFT) and quantum fluid dynamics (QFD) [7], to study mainly the TD changes in the electron density of helium atom under a petawatt laser We employ a *single* equation, a generalized non-linear Schrodinger equation (GNLSE) for many-electron systems (see below), derived earlier [8] and applied to helium atom [9–11], neon atom [11] and hydrogen molecule [12] For the calculations reported in this paper, a two-dimensional cylindrical grid of appropriate size has been employed whereas earlier works, also based on the GNLSE, had used either a limited grid [9,10] or a one-dimensional grid [11] Note that the GNLSE is a non-linear response theory in that it yields the TD electron density to all orders of change under the strong external perturbation. It also permits realistic single-system calculations unlike several earlier interesting calculations on model systems [13–15].

Since the formalism and a numerical method of solving the GNLSE have been described earlier [8–10,12], Section 2 describes the method of calculation briefly Section 3 discusses the results while Section 4 makes a few concluding remarks.

2. Method of Calculation

The GNLSE is given by (atomic units employed throughout this paper)

$$i\frac{\partial\psi(\boldsymbol{r},t)}{\partial t}=\left[-\frac{1}{2}\nabla^2+V_{\text{eff}}(\rho;\boldsymbol{r},t)\right]\psi(\boldsymbol{r},t) \tag{1}$$

where $\psi(\boldsymbol{r},t)$ is the hydrodynamical "wave function" (see, *e.g.*, [7]) from which the electron density $\rho(\boldsymbol{r},t)$ is obtained as $\rho(\boldsymbol{r},t)=|\psi(\boldsymbol{r},t)|^2$. The effective potential V_{eff} (ρ;

r t) comprises both classical and Coulomb terms It is expressed as a sum of potential terms representing electron-nuclear Coulomb attraction, interelectronic Coulomb repulsion, exchange and correlation interactions, interaction with an external field (in the present case, a laser field) and a non-classical kinetic energy correction term which vanishes for one-electron systems and two-electron Hartree-Fock systems (in the case of helium atom, this correction term is neglected) However, it makes a significant contribution for systems containing more than two electrons For one- and two-electron systems, eq (1) reduces to the TDSE and TD Kohn-Sham equations respectively It bears only a superficial resemblance to the Gross-Pitaevskii (GP) equation [16,17] for Bose-Einstein condensate but is actually more complicated than the GP equation due to the occurrence of non-integer powers of $\psi(\boldsymbol{r}, t)$ and an integral operator

Expressions for the various potential terms in V_{eff} $(\rho, \boldsymbol{r}, t)$ have been given earlier [12] The exchange contribution for a given density has been calculated exactly [8–10] For the correlation contribution, a local Wigner-type functional [12] has been employed, this functional yields excellent correlation energies for ground as well as excited states of atoms and molecules [12,18]

The laser potential has been taken in a classical, linearly polarized form, *viz*,

$$\delta E_{\text{laser}}[\rho]/\delta\rho = - E(t)\, z \tag{2}$$

where z is the direction of the applied laser electric field $E(t)$, given by

$$E(t) = E_0 f(t) \sin(\omega_L t) \tag{3}$$

In eq (3), ω_L is the laser frequency (a 1064 nm laser has been employed in the present work, with ω_L = 0 042823 a u and intensity $I = 1 \times 10^{15}$ W cm^{-2}), E_0 is the peak electric field given by $E_0 = (8\pi I/c)^{1/2}$, c being the speed of light, $f(t)$ is a dimensionless, linear ramp function which reaches its peak value of unity at the end of five optical cycles, *i e*,

$$f(t) = \begin{cases} t/t_0, & t < t_0 \\ 1, & t \geq t_0 \end{cases} \tag{4}$$

where t_0 = 733 594 a u (5 optical cycles) The ramp function helps the system take on the strong perturbation gradually instead of abruptly switching it on which is unrealistic

Under the action of the above laser field, the unperturbed, spherically symmetric helium atom acquires cylindrical symmetry. A cylindrical coordinate system is therefore a natural choice for the atom-laser system. Taking the origin at the helium nucleus, the coordinates are $\tilde{\rho}, \tilde{z}$ and φ, where $0 \leq \tilde{\rho} \leq \infty$, $-\infty \leq \tilde{z} \leq \infty$, $0 \leq \varphi \leq 2\pi$ Taking $\tilde{\rho} = x^2$ as well as omitting terms involving $\partial/\partial\varphi$ and $\partial/\partial\varphi^2$ due to azimuthal symmetry, one can transform eq. (1) into a form [8–10,12] amenable to numerical

solution. However, the azimuthal angle φ is involved in integrations over the entire three-dimensional space.

The two-dimensional space grid has been discretized as follows :

$0 \leq x \leq 5.1$ (*i.e.*, $0 \leq \tilde{\rho} \leq 26.01$); $-25.0 \leq \tilde{z} \leq 25.0$

$x_l = \delta + (l - 1)h$; $l = 1, 2, \ldots, N_1$; $\delta = 1 \times 10^{-6}$

$\tilde{z}_m = \tilde{z}_0 + mh$; $m = 1, 2, \ldots, N_2$

$\tilde{z}_0 = -N_2 h$

where $N_1 = 51$, $N_2 = 501$ and $h = 0.1$; δ has been chosen to avoid the Coulomb singularity at the nucleus.

The time grid is chosen as $0 \leq t \leq 4134.1276$ a.u. (1 a.u. of time = 0.0241889 *fs* = 24.1889 *as*), *i.e.*, 100 *fs*. The time step size $\Delta t = 0.07164$ a.u., *i.e.*, 1.733 *as* The calculations cover 28 optical cycles, each optical cycle being completed in 2048 time steps, *i.e.* 146.7187 a.u. of time or 3548.96 *as*. Thus, for the present laser of a single frequency and intensity, eq. (1) has been solved more than 57,700 times, the solution each time being equivalent to a static electronic structure calculation. The above space-time grids have already been employed for the H_2 molecule to obtain very good results [12].

For solving eq. (1) to obtain the time-dependent electron density in cylindrical coordinates, a finite-difference scheme has been employed, followed by Peaceman-Rachford splitting and a modified Thomas algorithm (for computational details, see [8–10,12]). In order to take care of reflections from the grid boundaries for obtaining the correct ionization rate, the following mask function, with an index different from that in [12], has been employed :

$$\cos^{1/8}\left[\frac{\pi(x - x_{abs})}{2(x_{max} - x_{abs})}\right] \cos^{1/8}\left[\frac{\pi(\tilde{z} - \tilde{z}_{abs})}{2(\tilde{z}_{max} - \tilde{z}_{abs})}\right]$$

where $x_{abs} = 3.2$ and $x_{max} = 5.1$ while $\tilde{z}_{max} = 25.0$ and $\tilde{z}_{abs} = 5.0$.

For launching the real-time dynamical calculations at $t = 0$, the input is the ground-state density of the helium atom. For internal consistency, this is obtained from eq. (1) through evolution in imaginary time, using the same algorithm as for real time. This approach is akin to the diffusion quantum Monte Carlo method (for the method and its other applications, see [19] and references therein). The ground-state density of helium atom, obtained with this formulation, is a highly accurate value of –2.9033 hartree compared to the exact non-relativistic value of –2.9037 hartree [20]. Since electron correlation is included, this input electron density is obviously more accurate than the corresponding Hartree-Fock density; this ensures better accuracy for the calculated TD density. Note that a more sophisticated algorithm for both imaginary-

time and real-time dynamics, according to eq. (1), has been developed recently [21].

The total number of electrons as a function of time can be expressed as

$$N(t) = \int_0^{26.01} \int_{25}^{+25} \int_0^{2\pi} \rho(\tilde{\rho}, \tilde{z}, t)\tilde{\rho} d\tilde{\rho} d\tilde{z} d\varphi; \quad N(0) = 2 . \tag{5}$$

The decreasing values of $N(t)$ with increasing time indicate the progress of ionization. For simplicity, the ionization rate has been calculated as $[N(0) - N(t)]/t_f$, where t_f = 100 fs, for the entire duration of the interaction.

The TD induced dipole moment, created in the atom by the laser electric field along the $\tilde{z}$-direction (cylindrical axis), is given by

$$\mu_{\tilde{z}}(t) = \int_0^{26.01} \int_{25}^{+25} \int_0^{2\pi} \rho(\tilde{\rho}, \tilde{z}, t)\tilde{z}\tilde{\rho} d\tilde{\rho} d\tilde{z}\, d\varphi \ . \tag{6}$$

3. Results and discussion

Figure 1 depicts (i) the contours of the ground-state correlated electron density of the helium atom at t = 0, (ii) the TD laser electric field $E(t)$, (iii) the TD norm $N(t)$, and (iv) the TD induced dipole moment $\mu_{\tilde{z}}(t)$ of the helium atom. The oscillation frequency of the dipole moment is the same as that of the laser field. However, after the ramp is crossed, its magnitude shows gradual damping due to progressive ionization (see the $N(t)$ plot). The present $N(t)$ plot and the rate of ionization show excellent agreement with the $N(t)$ plot (depicted up to t = 1500 a.u.) and the ionization rate respectively, resulting from the TD Hartree-Fock calculations of Kulander [22]. The dipole moment plot, however, agrees with that of Kulander qualitatively but not quantitatively. The $N(t)$ plot has a "staircase" structure which is explained below in terms of the movement of the electron density.

Figure 2 reflects the spatial competition or "tug-of-war" between the nuclear field and the ramped laser field experienced by the electron density in the atom. While the nuclear field is generally larger than the laser field in regions close to the nucleus, the spatial competition between the two is quite interesting. The regions of space where the nuclear field and the laser field dominate separately are colour-coded as yellow and purple respectively while the red area denotes a boundary region where the two fields "balance" each other. In Figure 2 (top left), at the trough (t = 110.039 a.u.) of the first optical cycle (see $E(t)$ plot in Figure 1), the effect of the laser field is small and the red region dominates the computation grid. At the trough (t = 403.476 a.u.) of the third optical cycle, the laser field makes its presence noticeable showing both red and purple regions. At the trough (t = 696.914 a.u.) of the fifth optical cycle and at subsequent troughs, the dominance of the laser field (purple) covers most regions of the computer grid except a small region around the nucleus; the red region has shrunk considerably. Note that the shape and size of the region of nuclear dominance

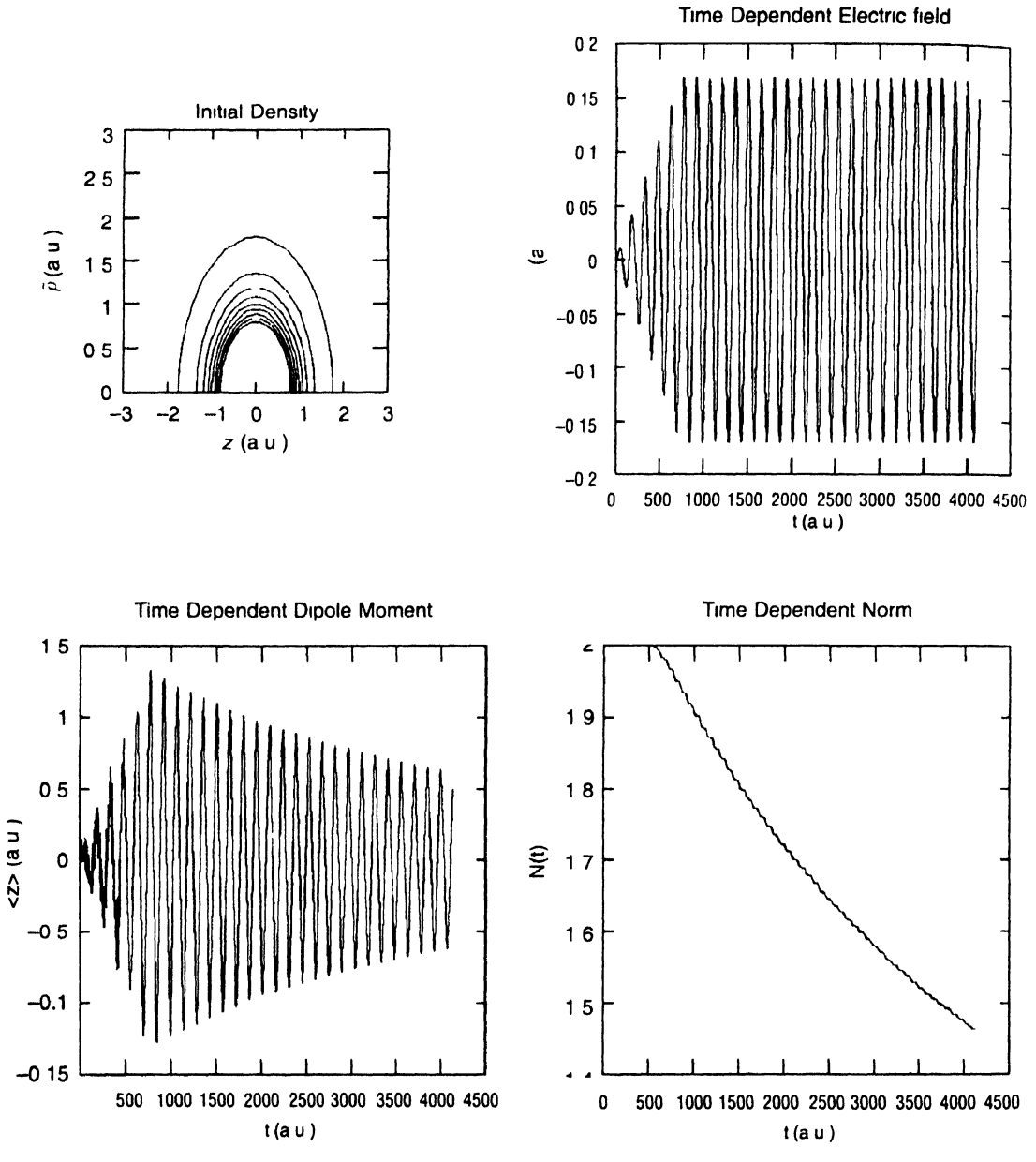

Figure 1. Ground-state helium atom density contours and TD laser electric field, norm $N(t)$ as well as induced dipole moment $<z> = \mu_z(t)$, in a u The values for the innermost and outermost density contours are 0.22 and 0 008 respectively The field and dipole moment plots are over 100 *fs*, covering 28 optical cycles

(yellow) do not change dramatically although this also shrinks somewhat along both $\tilde{\rho}$ and $\tilde{z}$ directions as the ramp is completed. These imply that, under the applied laser field, the atom would expand like a balloon, as we will see below.

Figure 3 depicts the TD electron density between the 14th and 15th optical

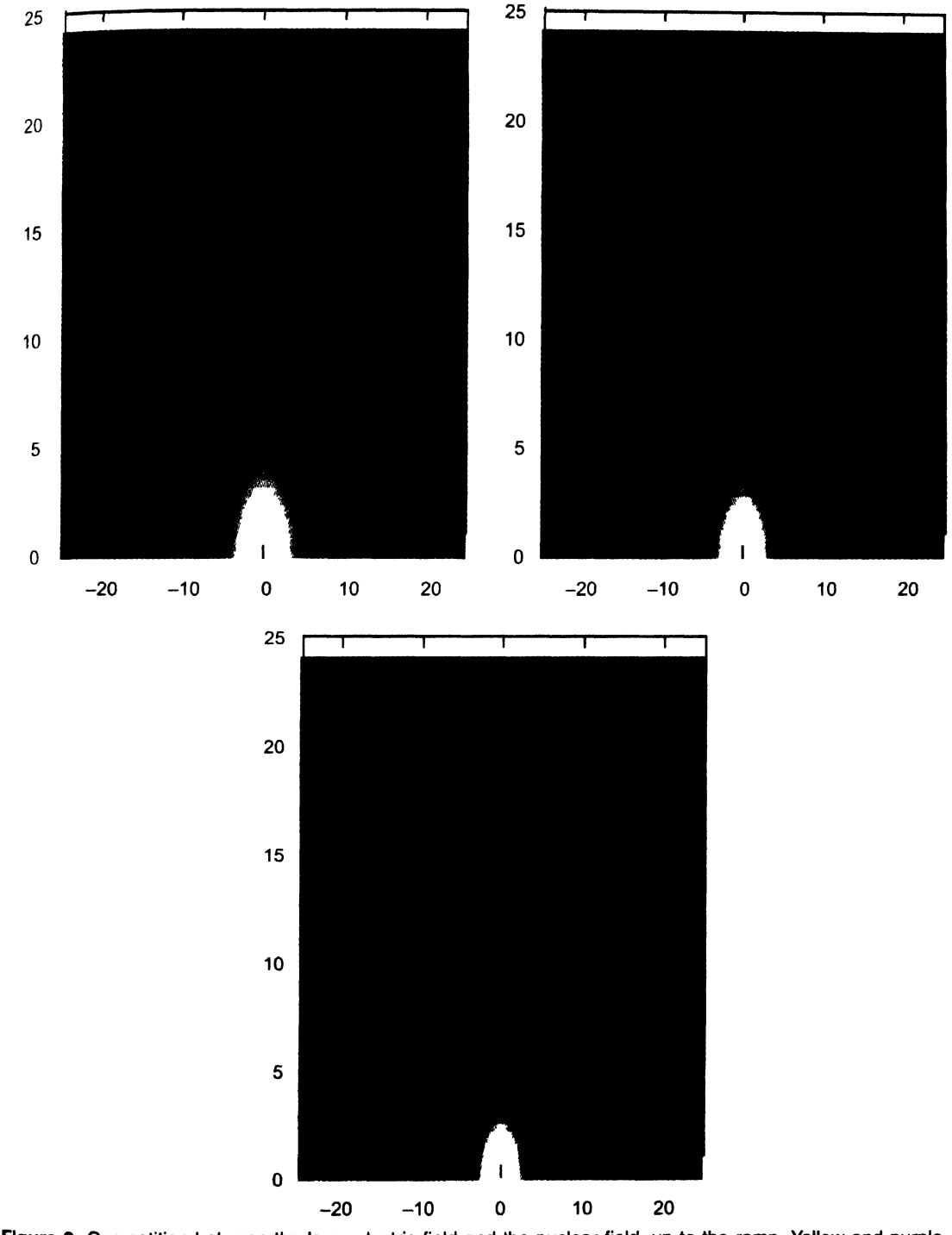

Figure 2. Competition between the laser electric field and the nuclear field, up to the ramp. Yellow and purple regions indicate nuclear dominance and laser dominance respectively, while the red region denotes a "balance" between the two fields. The ordinate and abscissa are $\tilde{\rho}$ and $\tilde{z}$. Top left, right and bottom pictures represent troughs of the 1st, 3rd and 5th optical cycles.

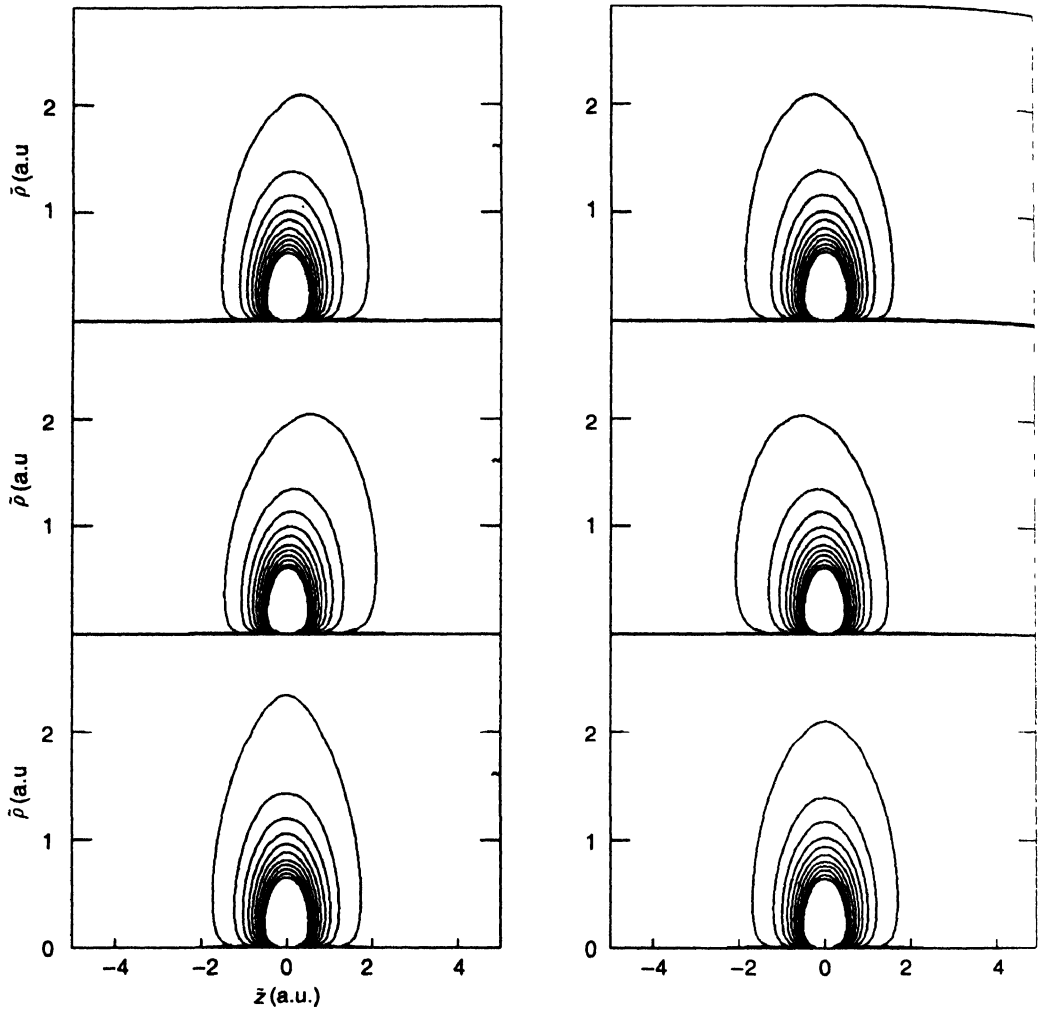

Figure 3. Electron density contours (a.u.) at different times between the 14th and 15th optical cycles. Panels from bottom left, clockwise denote n = 14.0, 14.2, 14.4, 14.6, 14.8 and 15.0, where $n = \omega_L t/2\pi$. The innermost and outermost density contours have the same values as in Figure 1. Note the *approximate* mirror-image symmetry of adjacent panels.

cycles (the n-th optical cycle is given by $\omega_L t/2\pi = n$) as "snapshots" at specific instants of time. Being under the dominance of the nuclear field (see Figure 2), the inner density contours are relatively less affected by the laser field. However, the outer density contours show pronounced left-right asymmetry; they are also seen to be pulsating in time. Such density changes over only one optical cycle are sufficiently large to be noticed visually. They also point to the accuracy of the present computations. For example, the panels in Figure 3 corresponding to each of the pairs n = 14.2, 14.8 and n = 14.4, 14.6 are *approximate* mirror images of each other while for n = 14 and 15 (cycles completed) the laser field vanishes and the electron density becomes symmetrical like the initial density. Note that, compared to the initial density, the

density at the end of the ramp spreads over greater space although ionization has not begun yet (Figure 1). Up to n = 15, nearly 31,000 time steps have been completed; thus, the present accuracy is quite satisfactory.

Since the asymmetry of electron density, depicted in Figure 3, reaches a maximum at the crest and trough of an optical cycle, the magnitude of the dipole moment is the largest at these times (Figure 1). As the TD electric field sweeps from right to left, the density also behaves in the same way. Furthermore, following Kulander [22], the "staircase" structure of the $N(t)$ plot (Figure 1) can be explained as follows : Because a significant amount of density is concentrated near the nucleus, a certain amount of time is necessary so that a part of the density can drift to the grid boundaries for ionization. During this time, the ionization rate remains negligibly small and $N(t)$ remains essentially unchanged, thereby creating the horizontal steps in $N(t)$. In other words, ionization occurs in sporadic bursts whereby the electron density oozes out of the computation grid mainly along the $\tilde{z}$ direction, the direction of the laser field.

An effective way to study the electron density changes, as a result of interaction with the laser field, is to look at the TD difference density $\Delta\rho(\boldsymbol{r}, t)$, defined as [8–10, 12]

$$\Delta\rho(\boldsymbol{r}, t) = \rho(\boldsymbol{r}, t) - \rho(\boldsymbol{r}, 0). \tag{7}$$

The difference density clearly reveals the accumulation or depletion of density at a point in space at a particular time. Figure 4 demonstrates that $\Delta\rho$ can be positive, negative or equal to zero. In every panel of Figure 4, the undulating dotted line corresponds to $\Delta\rho = 0$, lines above it correspond to $\Delta\rho > 0$ while lines below it correspond to $\Delta\rho < 0$. Thus, density is depleted from regions near the nucleus and accumulated elsewhere with interesting topography. The pronounced left-right asymmetry of the oscillating $\Delta\rho$ shows approximate mirror-image patterns for each of the pairs n = 14.2, 14.8 and n = 14.4, 14.6 (compare with Figure 3).

We now demonstrate that the present approach can also deliver results in the attosecond regime. We do this by depicting attosecond changes in the electron density as well as creating a train of attosecond laser pulses. Figure 5 shows the fluctuations in electron density that an observer, stationed at the point $\tilde{\rho}$ = 1.0, $\tilde{z}$ = 3.0 a.u., will experience. The frequency of the oscillating electron density at this point and other similar points in space is the same as that of the laser field. Since the chosen point is under nuclear dominance (Figure 2), a residual density lingers here. The attosecond variations in density over Δt = 20 a.u. = 483.78 *as* are shown more clearly in the inset of Figure 5. The corresponding density and difference density contours are depicted in Figure 6. Over a period of ~500 *as* or 0.5 fs, the changes in the contours of density and difference density are clearly discernible.

As mentioned before, under the influence of the laser field, the electron density expands considerably. When the density is scattered back by the nuclear field, large

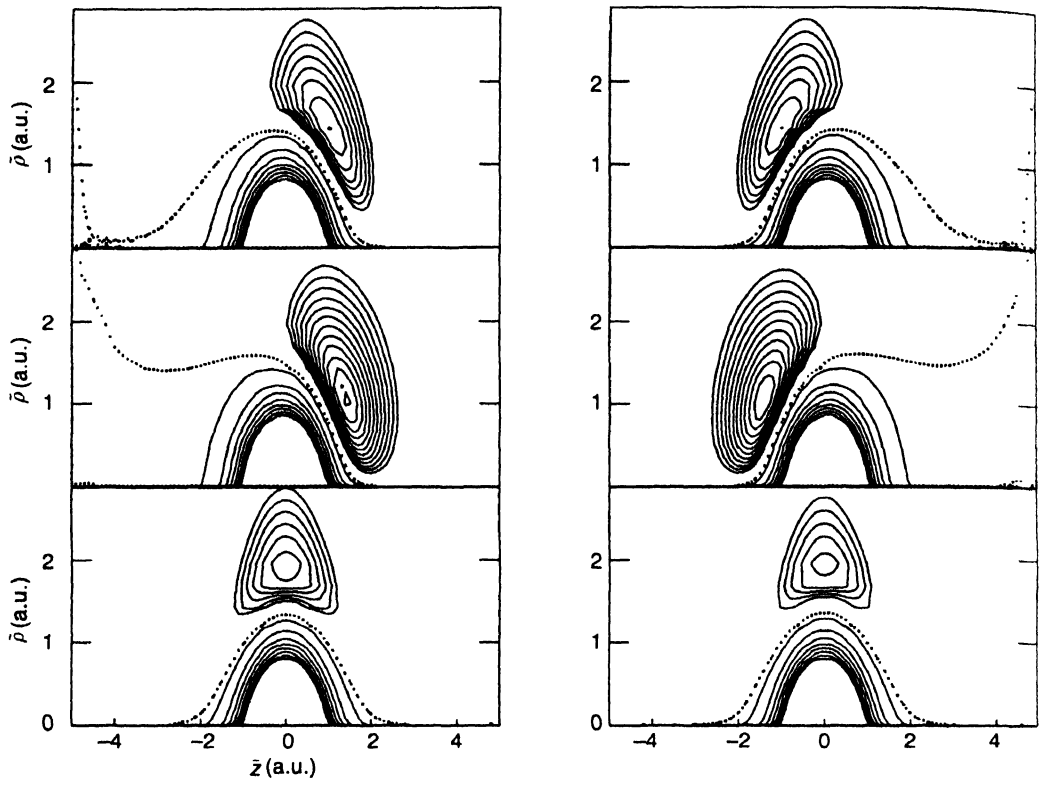

Figure 4. Difference density contours (a.u.) at different times between the 14th and 15th optical cycles (see also Figure 1). Panels from bottom left, clockwise represent $n = 14.0, 14.2, 14.4, 14.6, 14.8$ and 15.0, where $n = \omega_L t/2\pi$. The dotted line denotes $\Delta\rho = 0$. Contours above this line correspond to $\Delta\rho > 0$ (the value of the innermost contour is 0.005; the difference between successive contours is 0.0005) while contours below this line correspond to $\Delta\rho < 0$ (the value of the innermost contour is – 0.073; the difference between successive contours is 0.01). Note the approximate mirror-image symmetry of adjacent panels.

amounts of energy are released in the form of high-order harmonics of the incident laser frequency. Experimentally, up to 500 harmonics have been detected [2]. The HHG can be obtained as a power spectrum through a fast fourier transform of the TD induced dipole moment and has a well-known, characteristic appearance where a plateau occurs prominently [14]. The time structure of the HHG radiation can be obtained as the inverse fourier transform involving the second half of the plateau region in the HHG spectrum, *viz.*

$$I(t) = \left| \int^{\omega_1} D(\omega) e^{i\omega t} d\omega \right| \quad ; \omega_1 > \omega_0 \tag{8}$$

where

$$D(\omega) = \left| \int \mu(t) e^{-i\omega t} dt \right|^2 ; -\infty \leq \omega \leq \infty; \ \mu(-t) = \mu(t) . \tag{9}$$

In eq. (9), $\mu(t) \equiv \mu_{\hat{z}}(t)$, the TD dipole moment, ω_0 = 500, and ω_1 = 1,000.

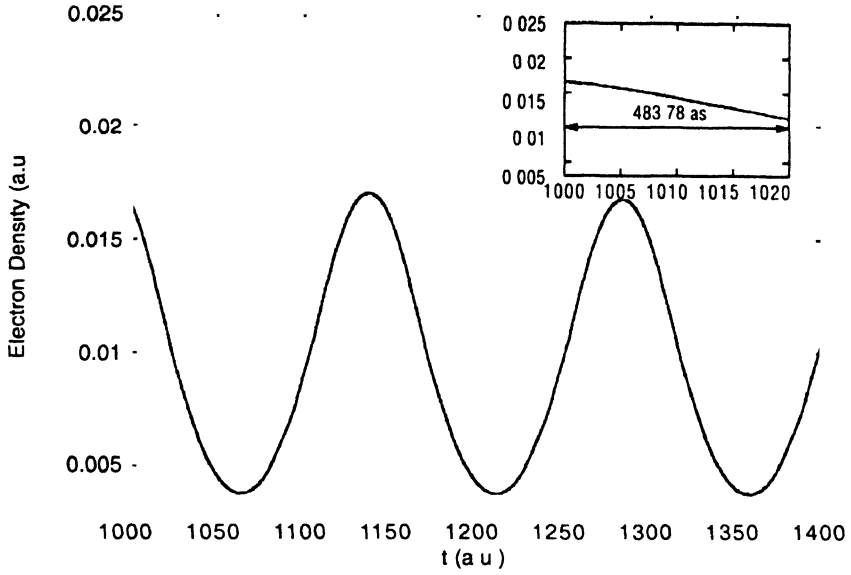

Figure 5. Density oscillations at a particular point (ρ = 1 0, z = 3.0 a u.) in space Inset shows the variation in density for 1000 $\leq t \leq$ 1020 a u., *i e.*, over 483 78 *as*

The time structure shows a train of narrow, attosecond XUV pulses of coherent radiation (Figure 7). The most intense pulse has a width of 98 *as* with $I = 4.5 \times 10^9$ W cm^{-2}. Such an attosecond pulse may be employed to capture the dynamics of electrons moving in attoseconds in a many-electron system. The pattern of the pulse train obtained in the present work is similar to that reported experimentally [2] by other workers who have generated XUV and X-ray pulses of width a few hundred attoseconds.

The physical reason for a very narrow pulse is as follows : The intensity of the emitted laser pulse is proportional to the kinetic energy of the electrons during scattering from the nucleus. The kinetic energy changes extremely rapidly, causing the pulse to have a duration in attoseconds.

4. Conclusion

By probing spatial electron density changes within a few hundred attoseconds during the atom-intense laser interaction and by generating an attosecond burst of coherent XUV radiation of satisfactory intensity, the present method of numerically solving the GNLSE has demonstrated its capability of probing the dynamics of electronic motions in atoms and molecules. It is realized that major experimental observations on such atom-laser interactions may be regarded as consequences of fluctuations of electron density in time and space. Needless to say, electron correlation plays a significant role in such fluctuations. Although the present formalism includes dynamic electron correlation, we have not explicitly demonstrated here the role such correlation plays in, *e.g.*, ionization; we hope to do so in future. Note that all doubly excited states of the helium atom are auto-ionizing due to electron correlation.

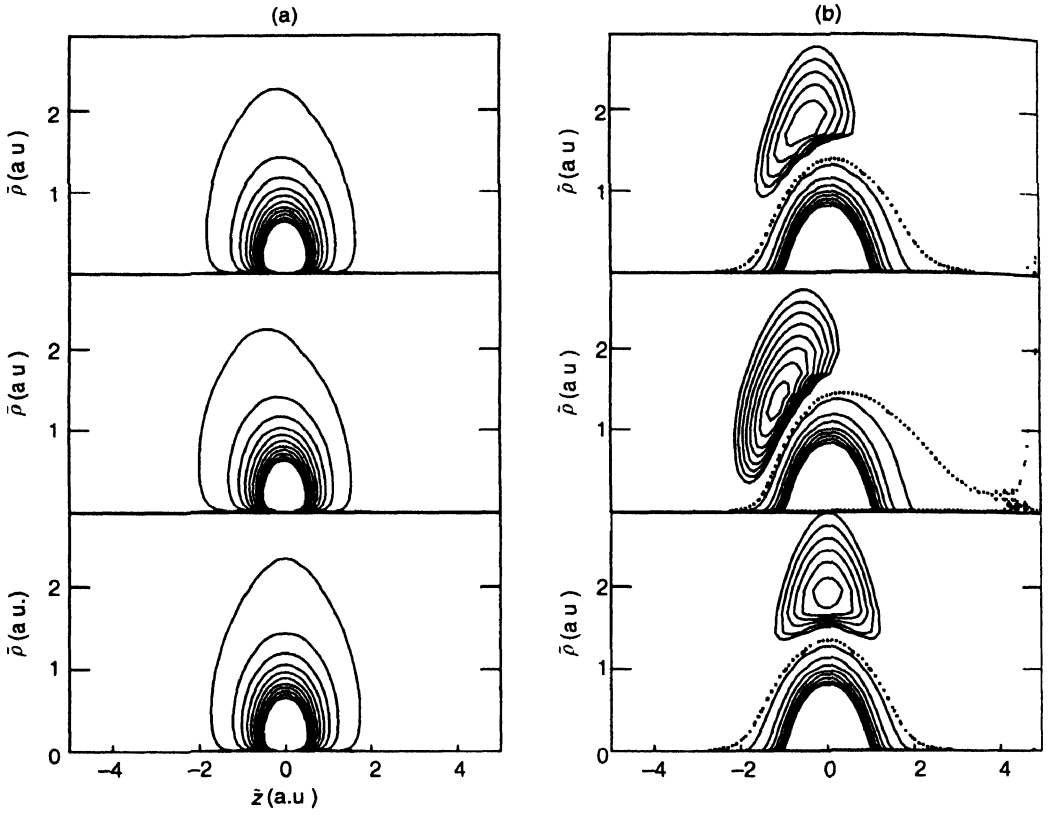

Figure 6. Attosecond variations (a u) in (a) density and (b) difference density, for $1000 \leq t \leq 1020$ a u , *i e* , over 483 78 *as* (see also Figure 5) Bottom pictures correspond to $t = 1000$ a u , middle pictures correspond to $t = 1010$ a.u and the top pictures correspond to $t = 1020$ a u For (a) and (b), contour values are as given in Figures 3 and 4 respectively

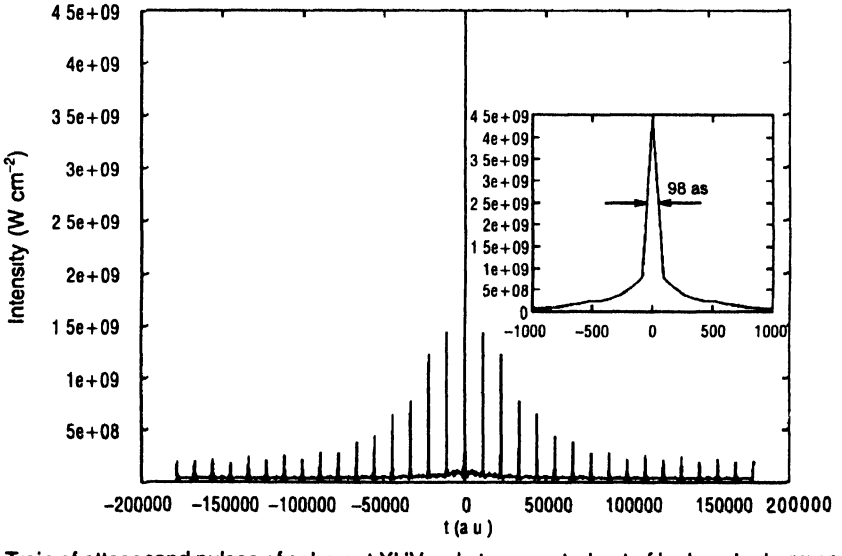

Figure 7. Train of attosecond pulses of coherent XUV radiation created out of high-order harmonics in the second half of the HHG plateau. Inset shows the profile of the most intense pulse of width 98 *as* and $I = 4.5 \times 10^9$ W cm^{-2}

An important assumption in the present calculations has been that the local Wigner correlation functional for static electron densities is also valid for TD densities. Although the present calculations do not indicate any serious violation of this assumption, one really requires universal kinetic, exchange and correlation functionals which would be valid for both static (ground and excited) and dynamic electron densities of atoms and molecules.

Acknowledgment

MS thanks the SNBNCBS, Kolkata for financial support.

References

[1] P Corkum, M Ivanov and D Villeneuve (eds.) *Special Issue on the Tenth International Conference on Multiphoton Precesses* (2005); *J. Phys. B: At. Mol. Opt. Phys.* **39** (2006)

[2] A Scrinzi, M Yu Ivanov, R Kleinberger and D M Villeneuve *J. Phys. B: At. Mol. Opt. Phys.* **39** R1 (2006)

[3] B Piraux and K Rzazewski (eds.) *Super-Intense Laser-Atom Physics* (Dordrecht : Kluwer Academic Press) (2001)

[4] J Posthumus *Molecules and Clusters in Intense Laser Fields* (Cambridge : Cambridge University Press) (2001)

[5] D Batani, C J Joachain, S Martellucci and A N Chester (eds.) *Atoms, Solids and Plasmas in Super-Intense Laser Fields* (Dordrecht : Kluwer Academic Press) (2001)

[6] Y Mairesse, A de Bohan, L J Frasinski, H Merdji, L C Dinu, P Monchicourt, P Breger, M Kovacev, R Taieb, B Carré, H G Muller, P Agostini and P Salières *Science* **302** 1540 (2003)

[7] B M Deb and S K Ghosh in *The Single-Particle Density in Physics and Chemistry* (ed.) N H March and B M Deb (London : Academic Press) (1987)

[8] B M Deb and P K Chattaraj *Phys. Rev.* **A39** 1696 (1989)

[9] B Kr Dey and B M Deb *Int. J. Quant. Chem.* **56** 707 (1995)

[10] B Kr Dey and B M Deb *Int. J. Quant. Chem.* **70** 441 (1998)

[11] A K Roy and S I Chu *Phys. Rev.* **A65** 043402 (2002)

[12] A Wadehra and B M Deb *Eur. Phys. J.* **D39** 141 (2006)

[13] D G Lappas and R Van Leewen *J. Phys. B: At. Mol. Opt. Phys.* **31** L249 (1998)

[14] A Wadehra, Vikas and B M Deb *J. Chem. Phys.* **119** 6620 (2003)

[15] M Lein and S Kümmel *Phys. Rev. Lett.* **94** 143003 (2005)

[16] E P Gross *Nuovo Cim.* **20** 454 (1961)

[17] L P Pitaevskii *Sov. Phys.-JETP* **13** 451 (1961)

[18] R Singh and B M Deb *Phys. Rep.* **311** 47 (1999)

[19] A K Roy, N Gupta and B M Deb *Phys. Rev.* **A65** 012109 (2002)

[20] E R Davidson, S A Hagstrom, S J Chakravorty, V M Umar and C F Fischer *Phys. Rev.* **A44** 7071 (1991)

[21] A Poddar and B M Deb *J. Phys. A : Math. Theor.* **40** 5981 (2007)

[22] K C Kulander *Phys. Rev.* **A36** 2726 (1987)